P H Y S I C A L   R E V I E W   L E T T E R S

Ring Polymers in the Melt State: The Physics of Crumpling

Angelo Rosa[*]

SISSA - Scuola Internazionale Superiore di Studi Avanzati, Via Bonomea 265, 34136 Trieste, Italy

Ralf Everaers[†]

*Laboratoire de Physique et Centre Blaise Pascal, École Normale Supérieure de Lyon,
CNRS UMR5672, 46 allée d'Italie, 69364 Lyon, France*

The conformational statistics of ring polymers in melts or dense solutions is strongly affected by their quenched microscopic topological state. The effect is particularly strong for nonconcatenated unknotted rings, which are known to crumple and segregate and which have been implicated as models for the generic behavior of interphase chromosomes. Here we use a computationally efficient multiscale approach to show that melts of rings of total contour length L_r can be *quantitatively* mapped onto melts of interacting lattice trees with gyration radii $\langle R_g^2(L_r)\rangle \propto L_r^{2\nu}$ and $\nu = 0.32 \pm 0.01$.

Similar to macroscopic strings tied into knots, the (Brownian) motion of polymer chains is subject to topological constraints: they can slide past each other, but their backbones cannot cross [1,2]. For *linear* chains, entanglements are transient and irrelevant for the equilibrium statistics: chains with a contour length exceeding the material specific Kuhn length, $L \gg l_K$, show Gaussian behavior with mean-square end-to-end distances $\langle R^2(L)\rangle = l_K L$. The only effect of the constraints is to slow down the chain dynamics beyond a density dependent entanglement (contour) length, L_e, a corresponding spatial distance or "tube" diameter, $d_T \propto \sqrt{l_K L_e}$, and a characteristic entanglement time, τ_e [3,4]. For loosely entangled systems, which are flexible at the entanglement scale, $L_e \approx (20/(\rho_K l_K^3))^2 \gg l_K$ [5–7], where ρ_K is the number density of Kuhn segments.

The situation is different for *unlinked* polymer melts or solutions, where the chain conformations have to respect (long-lived) *global* constraints enforcing the *absence* of topological knots and links [8]. Experimentally prepared systems of this type have interesting materials properties [9,10]. With large (interphase) chromosomes [11–17] the most prominent representatives are probably found in biological systems. In this case, the relaxation times for the topological state may be of the order of centuries [12,18], making the knot- and link-free state sufficiently long lived to merit attention. The best studied and yet still controversial [15] example are melts of nonconcatenated unknotted ring polymers. Values for the characteristic exponent ν relating the average-square gyration radius and total contour length $\langle R_g^2(L_r)\rangle \propto L_r^{2\nu}$ of proposed models range from $\nu = 1/4$ for ideal lattice trees or animals [19,20], $\nu = 1/3$ for crumpled globules [21], Hamiltonian paths [13,22], and interacting lattice trees [19,23]; $\nu = 2/5$ [24] from a Flory argument balancing the entropic cost of compressing Gaussian rings, and the unfavorable overlap with other chains (recently

refined to $\nu = 1/3$ for the asymptotic behavior [25]); to $\nu = [1 - 1/(3\pi)]/2 \approx 0.45$ [26], and $\nu = 1/2$ for Gaussian rings, rings folded into linear ribbons [27], and swollen lattice trees [28]. There is now strong numerical evidence [14,29–33] for a crossover to an asymptotic $\nu \approx 1/3$ regime around $Z_r \equiv L_r/L_e = 10$ [33]. But it is still not clear, which "strategy" the rings "adopt" to maximize the entropy of the solution.

In the following, we present results from a multiscale approach allowing us to identify the underlying physics and to access significantly larger system sizes than previous studies [14,29–33]. At the fiber level, we use molecular dynamics (MD) simulations of a bead-spring model for 30 nm chromatin fibers (see Ref. [12] and the Supplemental Material [34]). With $Z_r = 115$ our largest MD equilibrated rings are comparable in effective size to those of other recent computational studies [14,29–33]. In addition, we investigate a wide range of theoretically inspired and computationally much more efficient lattice models for the large scale behavior (Fig. 1). These models (studied using Monte Carlo simulations for ring sizes up to $Z_r = 900$) are discretized on the Kuhn scale of the fiber model, allowing us to "fine grain" results to corresponding off-lattice conformations of *nonconcatenated and unknotted* rings for the fiber model (see Supplemental Material [34]). The various models provide us with a sufficient range of qualitatively different initial states (Fig. 1) to validate the proper equilibration of our MD simulations [14] [see Fig. 2(a) vs its inset]. Moreover, by comparing identical observables for MD equilibrated target systems and model derived ensembles, we automatically account for numerical prefactors and crossovers in the test of the underlying physical ideas (Figs. 2 and 3). To adapt a well-known quote from Feynman, it is by attempting to construct equilibrated systems that we test our understanding of the factors controlling them.
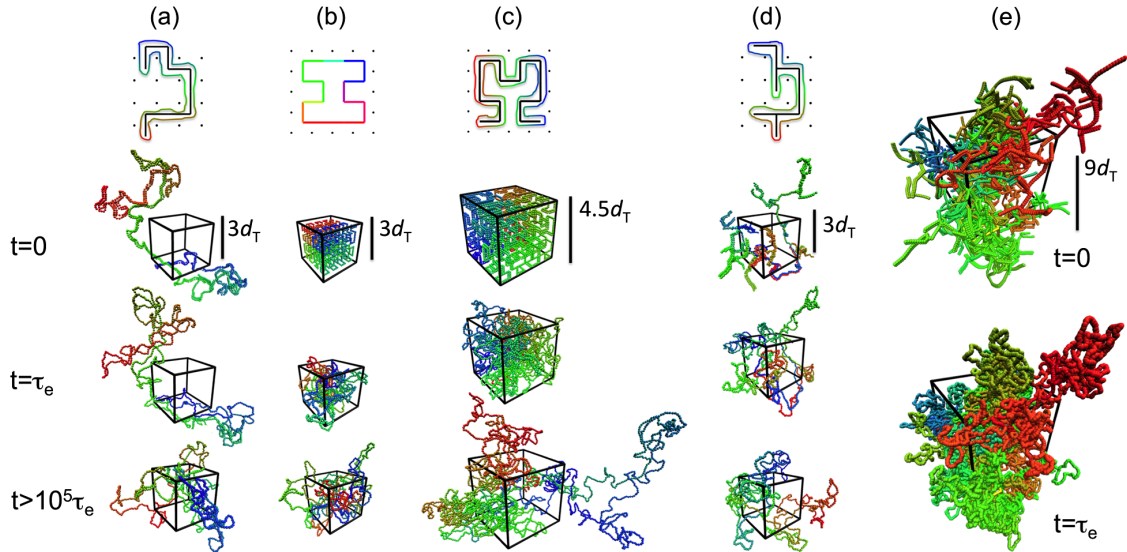
FIG. 1 (color online). Ring conformations derived from lattice models at various stages of MD equilibration. Top row: schematic view with dots representing vertically oriented sections of other chains or topological obstacles. Second row: at the beginning of MD simulation, $t = 0$; third row: after local MD equilibration on the entanglement scale, $t = \tau_e$; bottom row: after complete MD equilibration, $t \geq 10^5 \tau_e$. Columns: (a) Ribbon conformation with $Z_r = 38$ constructed around a linear random walk. (b) Ring conformation with $Z_r = 38$ following a space-filling Moore curve. (c) Ribbon conformation with $Z_r = 115$ constructed around an unbranched path following a space-filling Hilbert curve. (d) Ribbon conformation with $Z_r = 38$ constructed around an ideal lattice tree. (e) Ribbon conformation with $Z_r = 900$ constructed around a randomly branched tree from a lattice tree melt (only model configurations at $t = 0$ and $t = \tau_e$ are shown). Boxes indicate the volume, $V = (L_r/l_K)/\rho_K$, available to one ring. Following [13] we have used a color code linked to the monomer index. For details, please zoom into the electronic version of this figure.

Theoretical descriptions of ring melts have either associated the strength of the topological interactions with the threadable volume [24,25] or the threadable surface [19,20,27,28] that rings present to each other. Both approaches correctly predict the density dependence of the entanglement scale [7,24]. By taking the limit of zero threadable surface, proposals of the second type are easily translated into algorithms for constructing putative equilibrium states. Consider the idea [27], that ring polymers might fold into linear ribbons to freely thread between each other or between topological obstacles [Figs. 1(a)], while adopting noncompact ($\nu = 1/2$), spatially overlapping configurations. From a computational point of view, it is straightforward to assemble such solutions by randomly superimposing chains with random walk statistics and locally "pushing off" overlapping monomers [36]. In a second step, we construct bead-spring ring conformations as tightly closed ribbons along the contour and within the molecular volume of these chains (see Supplemental Material [34]). By construction, the rings are neither knotted nor topologically linked. The conformational statistics can be tuned to be in almost perfect agreement with the corresponding (open) Gaussian rings with $\langle R^2(L) \rangle = l_K L(1 - L/L_r)$ [Fig. 1(a) and S1 in the Supplemental Material [34]]. For ring sizes up to a few entanglement lengths, long (up to $\approx 10^4 \tau_e$) MD equilibration runs (see Table SIIIA in [34] for details) hardly affect the conformational statistics. However, larger rings undergo substantial shrinking and changes of shape (Figs. 1(a) and 2(a), and Table SIIIB in [34]).

A very different picture arises from the analogy to "crumpled globule" [21] conformations resulting from the collapse of swollen (and hence nearly knot free [37,38]) polymer chains, when solvent conditions are rapidly switched from good to poor [39]. Rapid mechanical confinement leads to similar, albeit also not particularly stable or well-defined states [40,41]. Constructing melt states from nonoverlapping crumpled globules obviously avoids the formation of topological links between different rings. It is often argued that the essential features of the chain conformations are represented by unknotted fractal space-filling curves [13,21,22]. In this case, the ring dimensions can be directly inferred from the contour length density, $l_K \rho_K$, of the solution. For cubic unit cells and in entanglement units, the occupied volume equals $(6^{3/2}/20)d_T^3 Z$, where $d_T \equiv \sqrt{\langle R_g^2(L_e) \rangle} = \sqrt{l_K L_e/6}$ denotes the tube diameter. Admissible chain lengths are multiples of 8 of an elementary length Z_0, which follows from the mapping of the contour length density in the elementary cell of the fractal construct (see Supplemental Material [34]). Here we use the Moore curve, which is the loop version of the Hilbert curve [42,43] with identical local properties. We have constructed Moore conformations for rings of $Z_r = L_r/L_e = 5, 38, 307$ entanglement lengths using a recursive mathematical algorithm (Fig. 1(b) and the Supplemental Material [34]). As an intermediate between the first two models, we have constructed compact ribbon conformations, where the ribbon axis follows a
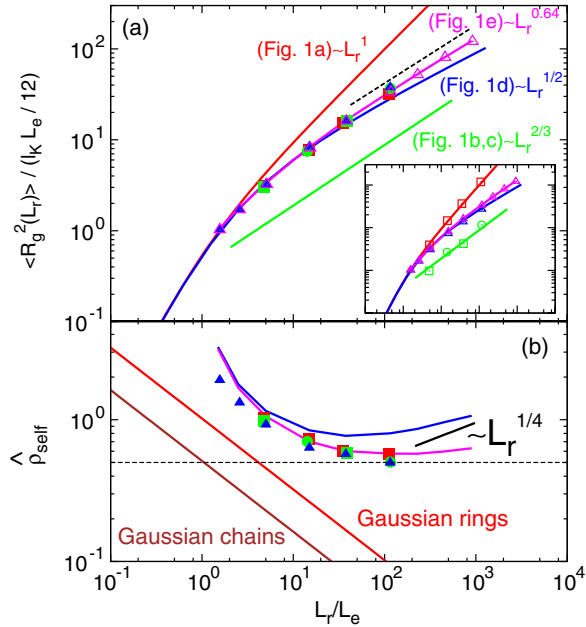
FIG. 2 (color online).   (a) Mean square gyration radius $\langle R_g^2 \rangle$ of rings of contour length L_r normalized to the square gyration radius of an ideal Gaussian ring of contour length $= L_e$. Solid lines: analytical and numerical predictions for the polymer models from Fig. 1. The dashed line marks the range where the exponent $2\nu = 0.64$ is observed. Filled symbols: $\langle R_g^2 \rangle$ after MD equilibration. (Inset) Open symbols: $\langle R_g^2 \rangle$ for the initial states of the simulations at $t = 0$. Magenta points for the interacting lattice tree model are also shown in the main panel. (b) Reduced self-density, $\hat{\rho}_{\text{self}}$, of chains at their centers of mass. Asymmetry ratios for Gaussian linear and ring polymers are $11.79 : 2.53 : 1.00$ and $6.14 : 2.28 : 1.00$ [35], respectively.

Hilbert curve instead of a random walk (Fig. 1(c) and see the Supplemental Material [34]). In this case admissible chain lengths are $Z_r = L_r/L_e = 14, 115, 926$ (see Supplemental Material [34]). Moore rings and Hilbert ribbons have similar conformational statistics [44]. The typical size grows like $\langle R^2(L) \rangle \sim L^{2/3}$ as long as $L \ll L_r$, but Hilbert ribbons are locally less crumpled. We have performed long (up to $\approx 5 \times 10^5 \tau_e$, Table SIIIA in [34]) MD simulations to equilibrate the systems with $Z_r \leq 115$. In all cases we observed substantial swelling and, hence, overlap of rings with their spatial neighbors [Figs. 1(b),1(c), and 2, and Table SIIIB in [34]].

A key insight [19,20,28] for the understanding of ring crumpling is the observation that rings, which are not entangled with fixed topological obstacles, can increase their entropy by folding into *branched* rather than linear ribbons [Fig. 1(d)]. In this case, the randomly branched ribbon axis resembles a lattice tree or lattice animal without internal loops. A number of exact results are available for the statistical properties of noninteracting, ideal systems [19,45–47]. In particular, $\nu = 1/4$ for $\lambda L \gg 1$, where λ is the branching probability per unit length [47] of the ribbon axis. By fitting the semiempirical expression combining Eq. S2 and Eq. S3 in [34] to the measured $\langle R_g^2 \rangle$ for the

first 4 equilibrated rings systems, we find that for $\lambda = (0.40 \pm 0.05)/l_K$ the predicted gyration radii are in excellent agreement with our MD results [Fig. 2(a)]. To allow for a detailed comparison, we have performed Monte Carlo simulations of randomly branched chains using the "amoeba" algorithm [48]. These were assembled into dense solution structures [36] before we built the corresponding branched ribbon conformations as models for the ring solutions (see Fig. 1(d) and the Supplemental Material [34]).

The bottom row of Fig. 1 illustrates that the final conformations of our MD runs resemble indeed the constructed branched ribbon conformations shown in column (d). In particular, the other unbranched starting conformations of our simulations all developed strongly branched loops. The quantitative analysis shows that for $Z_r = L_r/L_e \leq 10$ there are no significant differences between the conformations of rings equilibrated via MD and of rings we have derived from *ideal* lattice trees conformations [Fig. 2(a) and Table SIIIB in [34]]. In particular, we find excellent agreement for the ring gyration radii, $\langle R_g^2 \rangle = \langle \text{Tr}(S) \rangle$ [Fig. 2(a)], the asymmetry ratios of the average eigenvalues of the gyration or shape tensor, $S_{\alpha\beta} = (1/N) \sum_{i=1}^{N} (\vec{r}_{i\alpha} - \vec{r}_{\text{c.m.},\alpha})(\vec{r}_{i\beta} - \vec{r}_{\text{c.m.},\beta})$ (Table SIIIB in [34]), and the reduced self-density of the rings at their centers of mass (c.m.) $\hat{\rho}_{\text{self}}(L_r) \equiv \rho_{\text{self}}(\vec{r}_{\text{c.m.}}, L_r)/\rho = (\rho_{\text{chain}} \sqrt{(2\pi)^3 \det(S)})^{-1}$ [Fig. 2(b)]. Moreover, we find [44] that the ideal lattice tree model also describes the internal structure and dynamics [20,49,50] of larger rings on length scales up to $Z_r \sim 10$. Deviations become manifest on the scale of $Z_r \sim 100$ entanglements. As predicted in Ref. [19], the ring gyration radii enter a compact ($\nu \approx 1/3$) regime instead of crossing over to the characteristic $\nu = 1/4$ regime of strongly branched ideal lattice trees (Fig. 2 and Ref. [33] for a compilation of corresponding data from previous simulation studies).

The breakdown of the ideal behavior is best analyzed in terms of the predicted and observed reduced self-densities, $\hat{\rho}_{\text{self}}(L_r) \sim L_r/\langle R_g^2(L_r) \rangle^{3/2}$, using known [35] or our measured ratios of the eigenvalues of the gyration tensor. Consider first a solution of linear polymers with Gaussian statistics. We note that the standard entanglement length can be estimated from the condition $\hat{\rho}_{\text{self}}(L_e) \equiv 1/2$ [Fig. 2(b)]: fluctuations of a chain segment are subject to a (transient) topological constraint, if its center of mass coincides with the center of mass of a second segment of equal length. This observation is in excellent agreement with the binary character [51] of entanglements as revealed by a primitive path analysis [52]. For linear chains these constraints do not affect the equilibrium conformational statistics. Long chains strongly interpenetrate with $\hat{\rho}_{\text{self}}(L_r) = 0.5(L_e/L_r)^{1/2} = 0.5 Z_r^{-1/2}$, with the consequence that interactions are well described by mean-field models. The nearly [53] ideal Gaussian behavior is due to almost perfect screening [3]: any reduction in repulsive self-contacts in more extended single chain conformations is balanced by an equivalent increase in the number of contacts

with other chains. The situation is qualitatively different in melts of nonconcatenated ring polymers. As we have shown above, the conformational statistics is controlled by branching on the entanglement scale. According to the ideal lattice tree model, the self-density should reach a minimum of $\hat{\rho}_{\text{self}}(L_r) \approx 0.8$ for $L_r^*/l_K \approx 120$ or $Z_r^* \approx 30$ followed by an increase, $\hat{\rho}_{\text{self}}(L_r) \sim L_r^{1/4}$ for $Z_r \gg Z_r^*$. Instead, the observed self-densities stabilize around Z_r^* at the entanglement threshold $\hat{\rho}_{\text{self}} = 0.5 < 1$ [Fig. 2(b)]. In particular, the mutual overlap is drastically reduced compared to linear chains. The resulting reduced efficiency of screening leads to a breakdown of the ideal behavior in branched polymer solutions. While Flory arguments yield $\nu = 3/10$ [54] and $\nu = 4/13$ [23] for randomly branched polymers with quenched and annealed connectivity [55] in $d = 3$ dimensions, the chains are expected to swell asymptotically to $\nu = 1/d$ in both cases [19,23,47]. For comparison, $\nu = 1/2$ in $d = 3$ dimensions for self-avoiding lattice trees with unscreened excluded volume interactions [56].

To take molecular and topological [57] excluded volume interactions into account, we have introduced volume interactions into a multichain version of our Monte Carlo code for randomly branched polymers and run simulations for randomly branched chains of lengths $1 < Z_r < 900$ (for details, see the Supplemental Material [34]). Figure S3 in [34] demonstrates that starting from unbranched, random-walk-like configurations the chains reach more compact equilibrium configurations [panel (a)], while moving several times over distances corresponding to their average size [panel (b)]. Compared to the fiber model, the computational effort required for equilibration in the interacting lattice tree model is reduced by as much as 6 orders of magnitude (see Table SII in [34]). This allowed us to increase the investigated ring sizes from $Z_r = \mathcal{O}(100)$ (fiber MD) to $Z_r = \mathcal{O}(1000)$ (tree MC) and to simultaneously increase the system sizes from $M = \mathcal{O}(10)$ to $M = \mathcal{O}(100)$, the number of independent runs from $M = \mathcal{O}(1)$ to $M = \mathcal{O}(100)$ and the number of statistically independent configurations for the largest rings from $\mathcal{O}(10)$ (fiber MD, Table SIII in [34]) to $\mathcal{O}(1000)$ (tree MC, Table SI in [34]). Generalizations to coarser representations are straightforward and would increase the speed-up even further.

As demonstrated by Fig. 2 (magenta vs blue lines), excluded volume interactions lead to negligible deviations from the ideal behavior for tree sizes up to $Z_r = \mathcal{O}(10)$. Beyond this size, the interacting trees exhibit swelling. In agreement with the theoretical arguments, we observe for $30 \leq Z_r \leq 900$ an effective exponent of $\nu = 0.32 \pm 0.01$ (Fig. 2). Interestingly, the corresponding self-densities remain close to the entanglement threshold, $\hat{\rho}_{\text{self}} \approx 0.5 < 1$ [Fig. 2(b)], corresponding to a fractal structure where each part experiences the same amount of overlap and interactions with (or constraints due to) its spatial neighbors [22,58].

From the tree melt conformations we have again derived "fine-grained" ring melt structures [Fig. 1(e)]. The resulting conformations can be directly compared to the reliably
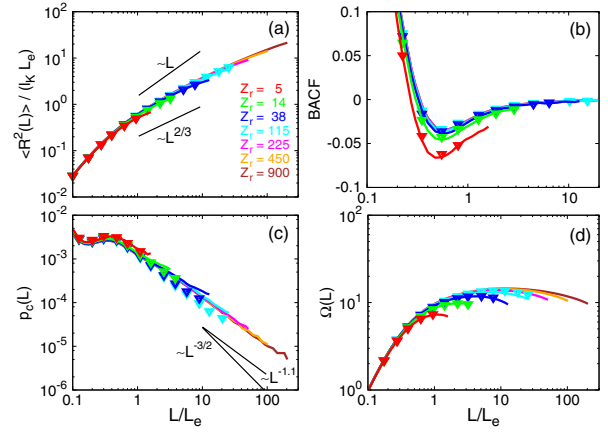

FIG. 3 (color online). Comparison of the conformational statistics of fully equilibrated rings (symbols) and of rings derived from lattice tree melt conformations (solid lines). (a) Mean-square internal distance, $\langle R^2(L) \rangle$. (b) Bond autocorrelation function (BACF). (c) Contact probability $p_c(L)$ taken at contact radius $= 2\sigma$, with $p_c(L) \sim L^{-1.11 \pm 0.01}$. (d) Overlap parameter. Data in panels (a), (c), and (d) extend up to 1/4 of the corresponding rings contour lengths.

equilibrated reference structures we have obtained by brute-force MD simulation for ring sizes $5 \leq Z_r \leq 115$. The agreement is excellent. This holds equally well for the ring gyration radii (magenta line and symbols in Fig. 2) and asphericities [44], as for measures of the internal structure (Fig. 3): (a) the mean-square spatial internal distance $\langle R^2(L) \rangle$; (b) the bond-angle correlation function $\text{BACF} = (1/N) \sum_{i=1}^{N} \langle \hat{t}_i \cdot \hat{t}_{i+L/\sigma} \rangle$, where $\hat{t}_i$ is the normalized bond vector between ring monomers i and $i + 1$; (c) the contact probability $p_c(L) \sim L^{-1.11 \pm 0.01}$ for $L/L_e > 10$, which is particularly relevant in the context of chromosome-chromosome interactions measured by HiC [13], and where we significantly extend the validity range of earlier results [32,59]; (d) the overlap parameter $\Omega(L) \equiv (\rho_K l_K / L) \langle R^2(L) \rangle^{3/2}$, which converges to the entanglement threshold, $\Omega \equiv 20$ [5–7]. In all cases, the modulo-N indexing due to the ring periodicity is implicitly assumed.

To conclude, we have used computer simulations to study dense solutions of nonconcatenated and unknotted ring polymers. Conceptually, we find strong evidence for the scenario that rings crumple by adopting lattice treelike ribbon structures characterized by randomly branched looping on the entanglement scale [19,20,28] and by an exponent $\nu = 1/3$ due to incomplete screening of excluded volume interactions [19,23] (but see [25] for an alternative explanation of the observed crossover disregarding the internal structure). Technically, we now dispose of a quantitative multiscale method for simulating knot- and link-free polymer solutions, which provides access to significantly larger system sizes than simulations at the fiber level alone. We note that with $M = 64$ rings of length $Z_r = 900 \sim 10^8$ DNA base pairs of our largest systems are comparable in size to the nucleus of a human cell [12], suggesting that it might become possible to include

generic topological constraints [11,12,15] into attempts to reconstruct or predict the three-dimensional folding of chromosomes in interphase nuclei [17,60].

[*]anrosa@sissa.it

[†]ralf.everaers@ens-lyon.fr

[1] S. F. Edwards, Proc. Phys. Soc. London **91**, 513 (1967).
[2] S. Prager and H. L. Frisch, J. Chem. Phys. **46**, 1475 (1967).
[3] M. Doi and S. F. Edwards, *The Theory of Polymer Dynamics* (Oxford University Press, New York, 1986).
[4] T. C. B. McLeish, Adv. Phys. **51**, 1379 (2002).
[5] T. A. Kavassalis and J. Noolandi, Phys. Rev. Lett. **59**, 2674 (1987).
[6] L. J. Fetters, D. J. Lohse, D. Richter, T. A. Witten, and A. Zirkel, Macromolecules **27**, 4639 (1994).
[7] N. Uchida, G. S. Grest, and R. Everaers, J. Chem. Phys. **128**, 044902 (2008).
[8] D. Rolfsen, *Knots and Links* (AMS Chelsea Publishing, Providence, Rhode Island, 1976).
[9] S. Rastogi, D. R. Lippits, G. W. M. Peters, R. Graf, Y. Yao, and H. W. Spiess, Nat. Mater. **4**, 635 (2005).
[10] M. Kapnistos, M. Lang, D. Vlassopoulos, W. Pyckhout-Hintzen, D. Richter, D. Cho, T. Chang, and M. Rubinstein, Nat. Mater. **7**, 997 (2008).
[11] A. Grosberg, Y. Rabin, S. Havlin, and A. Neer, Europhys. Lett. **23**, 373 (1993).
[12] A. Rosa and R. Everaers, PLoS Comput. Biol. **4**, e1000153 (2008).
[13] E. Lieberman-Aiden *et al.*, Science **326**, 289 (2009).
[14] T. Vettorel, A. Y. Grosberg, and K. Kremer, Phys. Biol. **6**, 025013 (2009).
[15] A. Y. Grosberg, Polym. Sci., Ser. C **54**, 1 (2012).
[16] M. Di Stefano, A. Rosa, V. Belcastro, D. di Bernardo, and C. Micheletti, PLoS Comput. Biol. **9**, e1003019 (2013).
[17] J. Dekker, M. A. Marti-Renom, and L. A. Mirny, Nat. Rev. Genet. **14**, 390 (2013).
[18] J.-L. Sikorav and G. Jannink, Biophys. J. **66**, 827 (1994).
[19] A. R. Khokhlov and S. K. Nechaev, Phys. Lett. **112A**, 156 (1985).
[20] S. P. Obukhov, M. Rubinstein, and T. Duke, Phys. Rev. Lett. **73**, 1263 (1994).
[21] A. Y. Grosberg, S. K. Nechaev, and E. I. Shakhnovich, J. Phys. (Les Ulis, Fr.) **49**, 2095 (1988).
[22] J. Smrek and A. Y. Grosberg, Physica (Amsterdam) **392A**, 6375 (2013).
[23] A. Y. Grosberg, Soft Matter **10**, 560 (2014).
[24] M. E. Cates and J. M. Deutsch, J. Phys. (Paris) **47**, 2121 (1986).
[25] T. Sakaue, Phys. Rev. Lett. **106**, 167802 (2011).
[26] M. G. Brereton and T. A. Vilgis, J. Phys. A **28**, 1149 (1995).
[27] J. Klein, Macromolecules **19**, 105 (1986).
[28] M. Rubinstein, Phys. Rev. Lett. **57**, 3023 (1986).
[29] M. Müller, J. P. Wittmer, and M. E. Cates, Phys. Rev. E **53**, 5063 (1996).
[30] M. Müller, J. P. Wittmer, and M. E. Cates, Phys. Rev. E **61**, 4078 (2000).
[31] J. Suzuki, A. Takano, T. Deguchi, and Y. Matsushita, J. Chem. Phys. **131**, 144902 (2009).
[32] J. D. Halverson, W. B. Lee, G. S. Grest, A. Y. Grosberg, and K. Kremer, J. Chem. Phys. **134**, 204904 (2011).
[33] J. D. Halverson, G. S. Grest, A. Y. Grosberg, and K. Kremer, Phys. Rev. Lett. **108**, 038301 (2012).
[34] See Supplemental Material at http://link.aps.org/supplemental/10.1103/PhysRevLett.112.118302 for details regarding the construction of the lattice models, and their fine-graining to the fiber level.
[35] M. Bishop and J. P. J. Michels, J. Chem. Phys. **84**, 444 (1986).
[36] R. Auhl, R. Everaers, G. S. Grest, K. Kremer, and S. J. Plimpton, J. Chem. Phys. **119**, 12718 (2003).
[37] A. Y. Grosberg, Polymer science Series A **51**, 70 (2009).
[38] C. Micheletti, D. Marenduzzo, and E. Orlandini, Phys. Rep. **504**, 1 (2011).
[39] P.-G. De Gennes, J. Phys. Lett. (Paris) **46**, 639 (1985).
[40] L. A. Mirny, Chromosome Res. **19**, 37 (2011).
[41] R. D. Schram, G. T. Barkema, and H. Schiessel, J. Chem. Phys. **138**, 224901 (2013).
[42] D. Hilbert, Math. Ann. **38**, 459 (1891).
[43] B. B. Mandelbrot, *The Fractal Geometry of Nature* (Freeman, New York, 1983), 2nd ed.
[44] A. Rosa and R. Everaers (to be published).
[45] B. H. Zimm and W. H. Stockmayer, J. Chem. Phys. **17**, 1301 (1949).
[46] P.-G. De Gennes, Biopolymers **6**, 715 (1968).
[47] M. Daoud and J. F. Joanny, J. Phys. (Paris) **42**, 1359 (1981).
[48] W. A. Seitz and D. J. Klein, J. Chem. Phys. **75**, 5190 (1981).
[49] S. T. Milner and J. D. Newhall, Phys. Rev. Lett. **105**, 208302 (2010).
[50] J. D. Halverson, W. B. Lee, G. S. Grest, A. Y. Grosberg, and K. Kremer, J. Chem. Phys. **134**, 204905 (2011).
[51] R. Everaers, Phys. Rev. E **86**, 022801 (2012).
[52] R. Everaers *et al.*, Science **303**, 823 (2004).
[53] J. P. Wittmer *et al.*, J. Stat. Phys. **145**, 1017 (2011).
[54] J. Isaacson and T. C. Lubensky, J. Phys. Lett. **41**, 469 (1980).
[55] A. M. Gutin, A. Y. Grosberg, and E. I. Shakhnovich, Macromolecules **26**, 1293 (1993).
[56] G. Parisi and N. Sourlas, Phys. Rev. Lett. **46**, 871 (1981).
[57] J. des Cloizeaux, J. Phys. Lett. (Paris) **42**, 433 (1981).
[58] M. Rubinstein (2012), talk in Leiden Conference on "Genome Mechanics at the Nuclear Scale", December 11.
[59] J. D. Halverson, K. Kremer, and A. Y. Grosberg, J. Phys. A **46**, 065002 (2013).
[60] H. Wong *et al.*, Curr. Biol. **22**, 1881 (2012).